WILEY-VCH

Homogeneous Doping of Substitutional Nitrogen/Carbon in TiO_2 Plates for Visible Light Photocatalytic Water Oxidation

Tingting Wu,[1,2] Ping Niu,[1] Yongqiang Yang,[1] Li-Chang Yin,[1] Jun Tan,[1] Huaze Zhu,[1,2] John TS Irvine,[3] Lianzhou Wang,[4] Gang Liu,[1,2] Hui-Ming Cheng[1,5]*

Ms T. T. Wu, Dr. P. Niu, Dr. Y. Q. Yang, Prof. L. C. Yin, Prof. J. Tan, Mr H. Z. Zhu, Prof. G. Liu, Prof. H. M. Cheng
Shenyang National Laboratory for Materials Science, Institute of Metal Research, Chinese Academy of Sciences, 72 Wenhua Road, Shenyang 110016, China

Ms T. T. Wu, Mr H. Z. Zhu, Prof. G. Liu
School of Materials Science and Engineering, University of Science and Technology of China, 72 Wenhua Road, Shenyang 110016, China

Prof. J. TS Irvine
School of Chemistry, University of St. Andrews, Fife, KY16 9ST, UK

Prof. L. Z. Wang
Nanomaterials Centre, School of Chemical Engineering and AIBN, The University of Queensland, St Lucia, Brisbane, QLD 4072, Australia

Prof. H. M. Cheng
Low-Dimensional Material and Device Laboratory, Tsinghua-Berkeley Shenzhen Institute, Tsinghua University, 1001 Xueyuan Road, Shenzhen 518055, China

E-mail: gangliu@imr.ac.cn

Keywords: homogeneous doping, photocatalyst, visible light, water splitting, topotactic transition

Abstract

Extending the light absorption range of wide-bandgap photocatalysts into the visible light region is significant in terms of fully harvesting and converting solar light. The desirable band-to-band redshift of the absorption edge of semiconducting binary metal oxides such as prototypical photocatalyst TiO_2 by doping has long been targeted but remains a challenge, up to date. Here, by taking the advantage of abundant one-dimensional diffusion channels with rhombus-like cross-sections along the c-axis in the crystal structure of titanium oxalate hydrate to promote the entrance of nitrogen dopant species into the bulk and subsequent thermal topotactic transition in an atmosphere of gaseous ammonia, the homogeneous doping of substitutional carbon/nitrogen for oxygen in the TiO_2 decahedral plates with a dominant anatase phase was obtained for the first time. The resultant $TiO_{2-x}(CN)_y$ with an unusual band-to-band visible light absorption spectrum can induce photocatalytic water oxidation to release oxygen under visible light irradiation. This study provides not only a promising visible light-responsive TiO_2 photocatalyst but also an important strategy for developing other solar-driven photocatalysts.

1. Introduction

Photocatalysis occurring on the surface of suitable semiconductors under light irradiation is a very promising technique of utilizing solar energy by inducing the decomposition of target molecules (i.e., H_2O, CO_2 and organic molecules). Developing visible light responsive photocatalysts has been actively pursued in order to fully utilize visible-light dominant solar light.[1-18] Stable metal oxide semiconductors with suitable electronic structures as promising photocatalysts usually suffer from their large bandgap of over 3 eV so that little visible light can be absorbed.[18-21] To overcome this bottleneck, various strategies, in particular anion doping,[22-25] have been attempted to change the electronic structures of metal oxides to narrow bandgap for the absorption of low energy photons. The mechanism of anion doping induced bandgap narrowing of metal oxides is that the substitutional anion dopants, such as boron, carbon and nitrogen with the smaller electronegativity than oxygen, can effectively elevate the maximum of original valence band that is dominated by O 2*p* states.[22, 26-28] It is established that, besides the species of the dopants, their spatially homogeneous distribution in the materials for the indispensable long-range interaction of the dopants with intrinsic bulk atoms is equally crucial in enabling the bandgap narrowing (a desirable band-to-band visible light absorption spectrum is formed in this situation).[23, 29, 30] However, numerous studies have suggested that these anion dopants tend to locate at the surface layer of metal oxides, particularly TiO_2,[19, 31, 32] so that only a low density of localized states are formed in the bandgap (an unfavorable shoulder-like visible light absorption spectrum is formed in this case). This limitation is intrinsically caused by the lack of favorable diffusion pathways for dopant species from surface to bulk of the materials when subject to post-treatment assisted doping, which restrains the realization of the homogeneous distribution of dopants. Developing the capability of controlling the spatially homogeneous distribution of suitable dopants in photocatalysts is, therefore, highly necessary but is far from satisfactory.

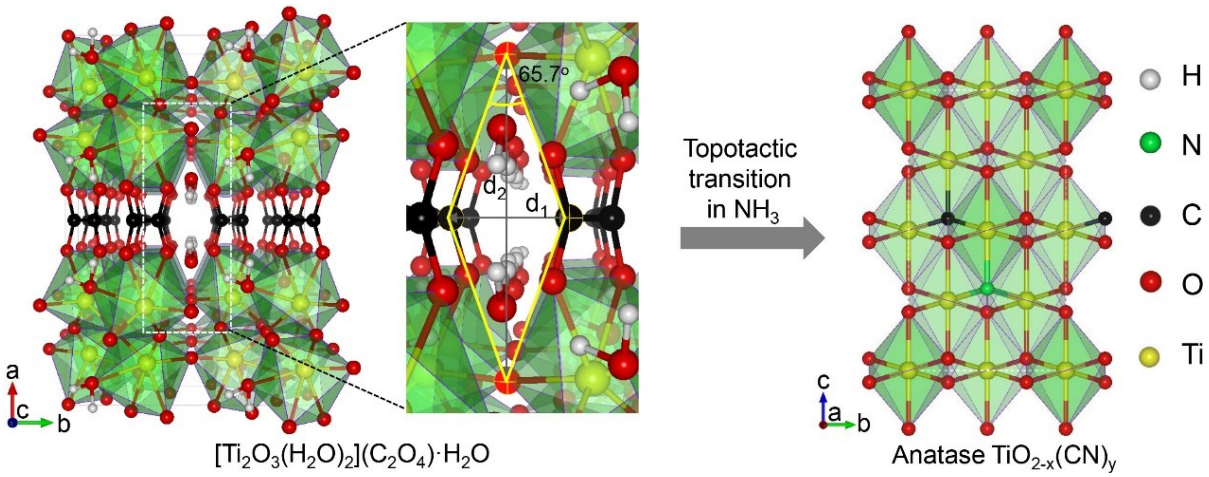

Figure 1. Schematic of the preparation of the homogenously nitrogen/carbon doped anatase TiO_2 from titanium oxalate hydrate by the thermal topotactic transition in an atmosphere of gaseous ammonia. The left panel is the supercell of titanium oxalate hydrate and the enlarged part showing the one-dimensional channels with a rhombus-like cross-section (d_1, 3.8 Å; d_2, 5.9 Å; the acute angle of the rhombus-like cross-section, 65.7°). The right panel is the unit cell of anatase TiO_2 with substitutional carbon and nitrogen for two oxygen atoms.

Although a layered structure with weak interlayer interaction is recognized to be useful for the facile diffusion of dopant species in the interlayer galleries to enable desired homogeneous doping (i.e., homogeneous nitrogen doping in $Cs_{0.68}Ti_{1.83}O_4$)[29], the fact of both a very limited number of metal oxides with a layered structure and the high confinement effect of the photogenerated charge carriers within the layers of these materials greatly impairs its practical application for developing efficient visible light driven photocatalysts.[33, 34] To address this challenge, it seems necessary to explore other unique microstructures that can facilitate homogeneous doping without impairing the transport properties of the photogenerated charge carriers. In this study, the unique atomic structure of a titanium oxalate hydrate ($Ti_2O_3(H_2O)_2(C_2O_4)$•H_2O) crystal, where the 5.6 Å thick conjugated layers of corner-sharing TiO_6 octahedra are interconnected by oxalate ions and water molecules are separately confined within the one-dimensional channels with rhombus-like cross-sections, are found to

be effective in enabling the homogeneous nitrogen/carbon doping during the thermal topotactic transition from titanium oxalate to $TiO_{2-x}(CN)_y$ in an atmosphere of gaseous ammonia, as schematically shown in **Figure 1**. The large spaces in these abundant one-dimensional channels are considered to play a key role in realizing homogenous doping by promoting the diffusion of NH_3 molecules and their thermal decomposition derivatives into the interior of the crystals. As a consequence of the homogeneous N/C doping, the resultant $TiO_{2-x}(CN)_y$ sample shows a strong band-to-band visible light absorption spectrum, and can induce photocatalytic water oxidation to produce oxygen under visible light irradiation.

2. Results and Discussion

The titanium oxalate hydrate crystals used were prepared by an aqueous precipitation reaction with titanium oxysulfate ($TiOSO_4 \cdot xH_2O$) as a titanium precursor and lithium oxalate ($Li_2C_2O_4$) as the ligand stabilizer of the titanium oxalate hydrate phase, according to the modified procedures.[35, 36] Scanning electron microcopy (SEM) image in **Figure 2a** shows that the uniform crystals of over two microns have a plate-like decahedral shape with flat basal/lateral surfaces and sharp edges. All diffraction peaks in X-ray diffraction (XRD) patterns (**Figure S1**, Supporting Information) of the sample are assigned to the orthorhombic phase of titanium oxalate hydrate (orthorhombic symmetry, space group C*mca*, a = 15.494 Å, b = 10.491 Å, and c = 9.700 Å),[37] and the strong and sharp peaks suggest the high crystallinity of the sample.

The $TiO_{2-x}(CN)_y$ particles derived from the thermal topotactic transition of titanium oxalate hydrate in the atmosphere of gaseous ammonia basically retain the original shape of the titanium oxalate particles as shown in Figure 2b. This is a typical result of the nature of the good conformality of the topotactic transition process, where two materials involved actually share the same building blocks like TiO_6 octahedron in this case. However, compared to the titanium oxalate hydrate particles, two changes are associated with the resultant $TiO_{2-x}(CN)_y$

particles. One is a certain volume shrinkage due to the release of water molecules and oxalate ions and crystal structure difference between two materials. The other is the large roughness of the basal surfaces and uneven lateral surfaces probably due to the reductive nature of NH_3 atmosphere. The reference TiO_2 sample (SEM image in **Figure S2**, Supporting Information) prepared by the topotactic transition at the same conditions but in air has a much similar shape to that of the titanium oxalate sample. Comparison of XRD patterns (**Figure S3**, Supporting Information) of two samples TiO_2 and $TiO_{2-x}(CN)_y$ indicates two features. One is that both samples have a dominant anatase phase and minor rutile phase, and the latter has additional minor brookite phase, which is also confirmed by the typical active modes of brookite TiO_2 in the Raman spectrum of $TiO_{2-x}(CN)_y$ (**Figure S4**, Supporting Information). The other is the much broader and weaker diffraction peaks of anatase phase in TiO_2 than that of $TiO_{2-x}(CN)_y$, indicating the lower crystallinity and/or smaller crystal grains in the $TiO_{2-x}(CN)_y$ plates. The polycrystalline nature of the plates is directly confirmed by the transmission electron microscopy (TEM) images of the thin sheets cut from one particle (Figure 2c and d). The measured lattice spacing of 3.52 Å can be assigned to the most stable low-index (101) planes of anatase TiO_2. Some disordered or lost-atoms containing micro-regions are formed largely because of the introduction of nitrogen/carbon heteroatoms and oxygen vacancies. In contrast to the TiO_2 samples derived from the thermal topotactic transition of titanium oxalate hydrate in air or argon that have nanoparticles with a size in tens of nanometers as building blocks, the $TiO_{2-x}(CN)_y$ plate is composted of the closely stacked nanoparticles with the size smaller than 10 nm. This is consistent with the result from their XRD patterns. It means that the refinement of the crystal grains of titanium oxalate hydrate during the thermal topotactic transition is sensitive to the gaseous atmosphere, and a reductive atmosphere leads to small nanoparticles and oxidative or inert atmosphere leads to large nanoparticles.

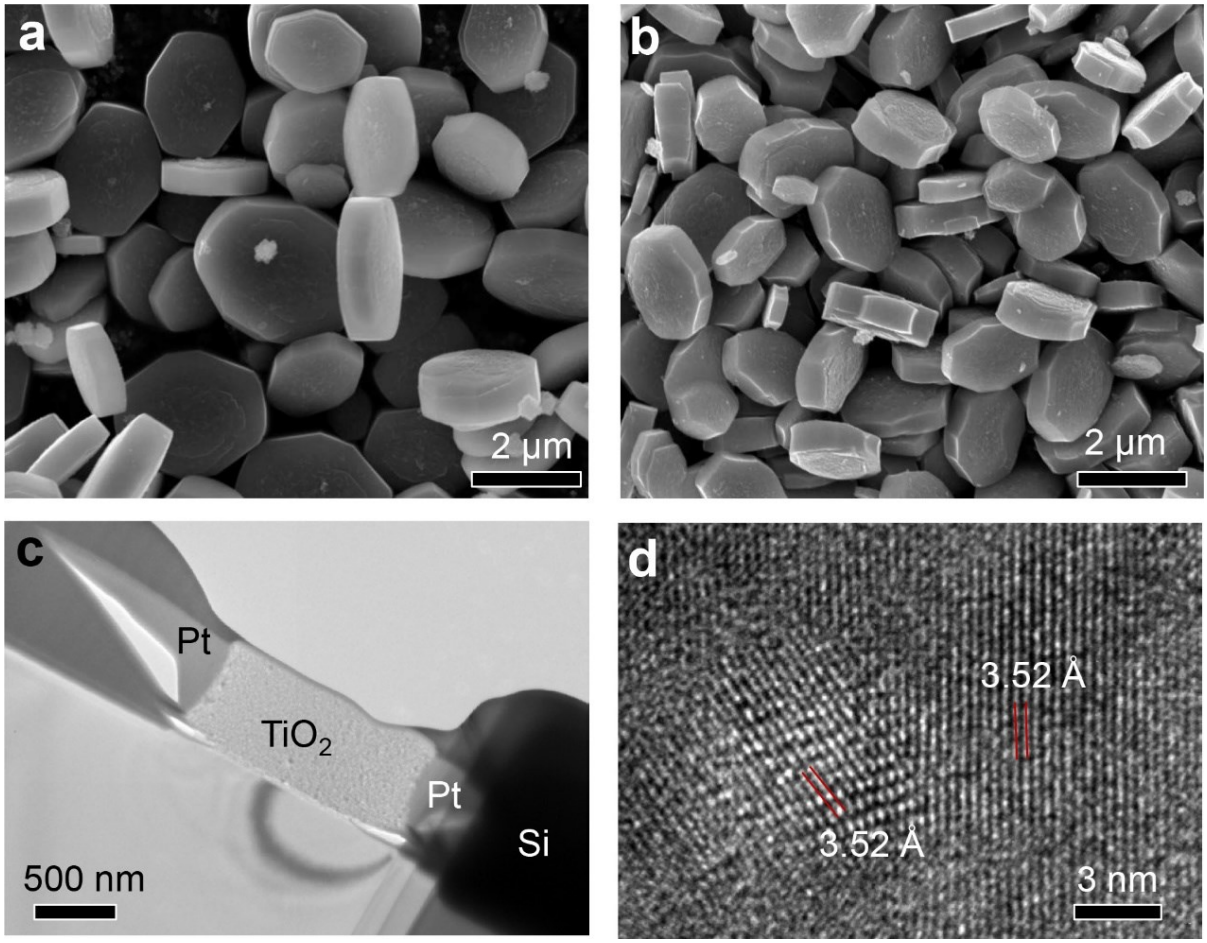

Figure 2. SEM images of (**a**) titanium oxalate hydrate sample, (**b**) $TiO_{2-x}(CN)_y$ sample obtained by heating the titanium oxalate sample at 550 ºC in the atmosphere of gaseous ammonia. (**c**) TEM image of a thin sheet cut from a $TiO_{2-x}(CN)_y$ particle supported on a Si wafer substrate. Prior to cutting by focus ion beam, the particles were fixed on the substrate by coating a platinum layer. (**d**) High resolution TEM image of the sample recorded from the typical region of the sheet in (c).

The spatial distribution and chemical state of carbon and nitrogen dopants in the $TiO_{2-x}(CN)_y$ decahedral particles were investigated by the combination of Energy Dispersive Spectrometer (EDS) elemental mappings and profiles, and X-ray photoelectron spectroscopy. Comparison of the elemental mapping images of carbon and nitrogen dopants with that of intrinsic Ti and O elements in a single particle in **Figure 3**a and b qualitatively suggests the

uniform distribution of both carbon and nitrogen dopants in the particle. The elemental profiles along the direction of the short side of the particle in Figure 3c and d semi-quantitatively confirm the homogeneous distribution of nitrogen and carbon in the particle. On the basis of the depth profiles of XPS spectra of N 1*s* and C 1*s* core electrons in Figure 3e and f, two major features are revealed. One is the successful incorporation of the substitutional nitrogen and carbon for oxygen in the form of Ti-N and Ti-C bonds in the TiO_2 particles, as indicated by the binding energy of 397.1 eV for N 1s core electrons and 281.8 eV for C 1s core electrons,[22, 36] respectively. Note that the strong C 1s signal at 284.8 eV arises from the adventitious carbon on the sample surface. The other is the double confirmation of the homogeneous location of nitrogen and carbon in the whole interior of the particles. The atomic ratio of N to Ti is determined to be around 5%. It is also noted that no obvious N 1s and C 1s signals are detected from the surface of the pristine sample, which is probably caused by the easy escape of nitrogen and carbon dopants from the top layer of the particles during the thermal topotactic transition. The dopant-free surface might play a positive role in stabilizing the $TiO_{2-x}(CN)_y$ sample as photocatalyst. All these results consistently show the homogeneous distribution of the substitutional nitrogen and carbon for oxygen in these plates as anticipated.

The success of using titanium oxalate hydrate as a precursor to prepare TiO_2 crystals with the homogeneous doping of nitrogen and carbon can be rationalized by the substantial role of the one-dimensional spaces in the crystal structure of titanium oxalate hydrate in facilitating the entrance of ammonia-related species into the material interior. As shown in Figure 1, the rhombus-like cross-section of the one-dimensional opening channel has a width of 3.8 Å (d_1) and length of 5.9 Å (d_2). Each unit cell contains one opening channel, so the density of the channels in the crystal is quite high. Considering the smaller experimental diameter of 3.64 Å of a NH_3 molecule than the width of 3.8 Å of the rhombus-like cross-section, the NH_3 molecules and their thermal decomposition species such as NH_2^- and NH^{2-} shall enter the

channels easily. The stored nitrogen species in the abundant channels can be a nitrogen source to *in situ* realize the homogeneous nitrogen doping in the topotactic transition of titanium oxalate hydrate. In contrast, if the precursor (i.e., amorphous titanium hydroxide or crystalline titanium dioxide) without similar channels for the entrance of nitrogen species into the bulk was used, only surface N doping that causes a small shoulder-like visible light absorption band can be realized. On the other hand, the atomically uniform distribution of carbon species as the intrinsic composition of titanium oxalate hydrate itself makes it possible to achieve carbon doping in the bulk of the resultant doped TiO_2.

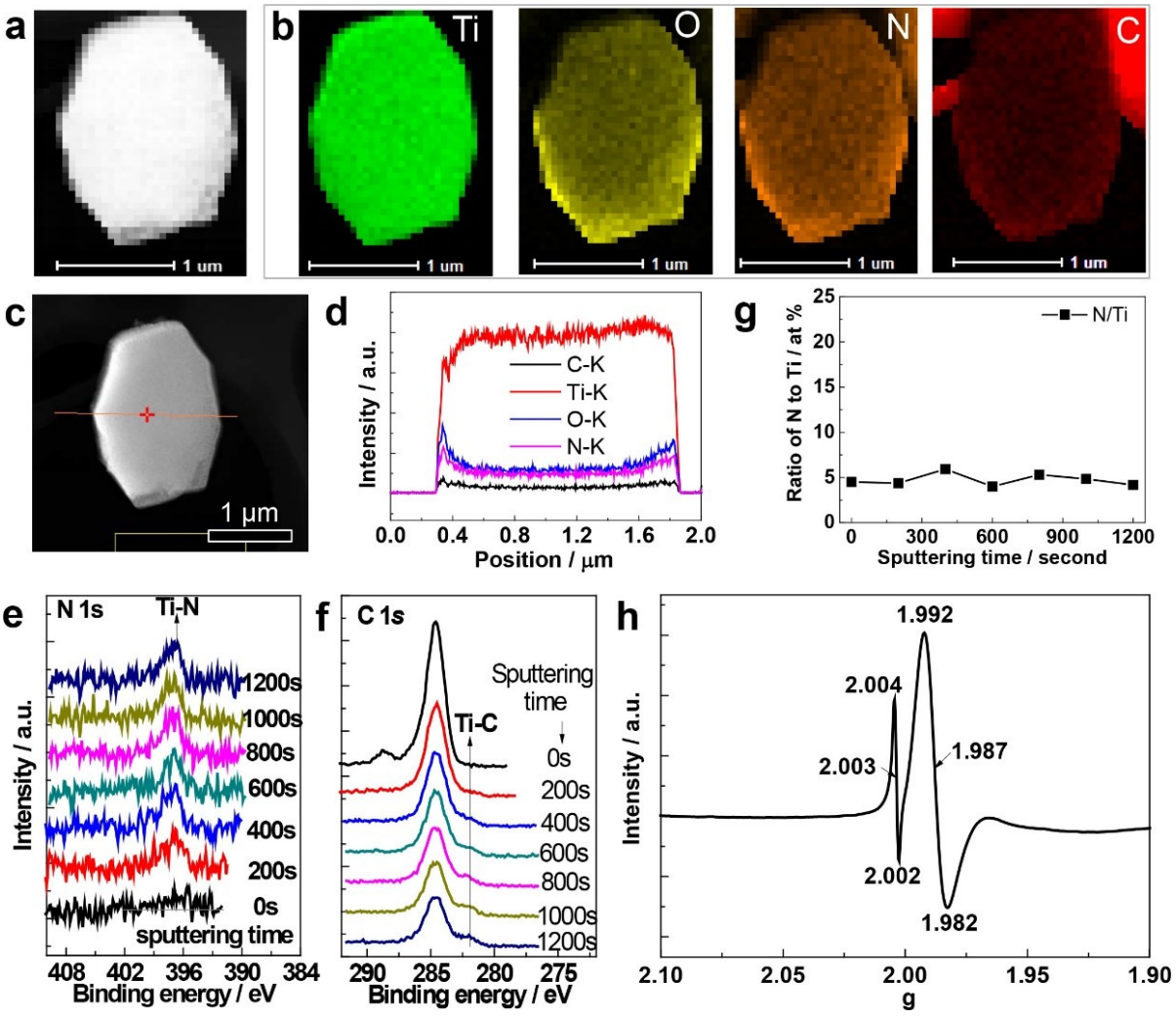

Figure 3. a, Scanning transmission electron microscopy (STEM) image of a $TiO_{2-x}(CN)_y$ particle. **b**, Ti, O, N and C element EDS mappings of the $TiO_{2-x}(CN)_y$ particle. **c**, High-angle

annular dark field (HAADF) STEM image of the $TiO_{2-x}(CN)_y$ particle marked with a red line that gives the scanning path to record elemental profiles of Ti, O, N and C-k in **d**. **e** and **f**, Ar ion sputtering time dependent profiles of N 1s and C 1s XPS spectra recorded from the $TiO_{2-x}(CN)_y$ sample. **g**, The atomic ratio of N to Ti in the $TiO_{2-x}(CN)_y$ sample as a function of Ar ion sputtering time. **h**, Electron spin resonance spectrum of the $TiO_{2-x}(CN)_y$ sample measured at 140 K in dark.

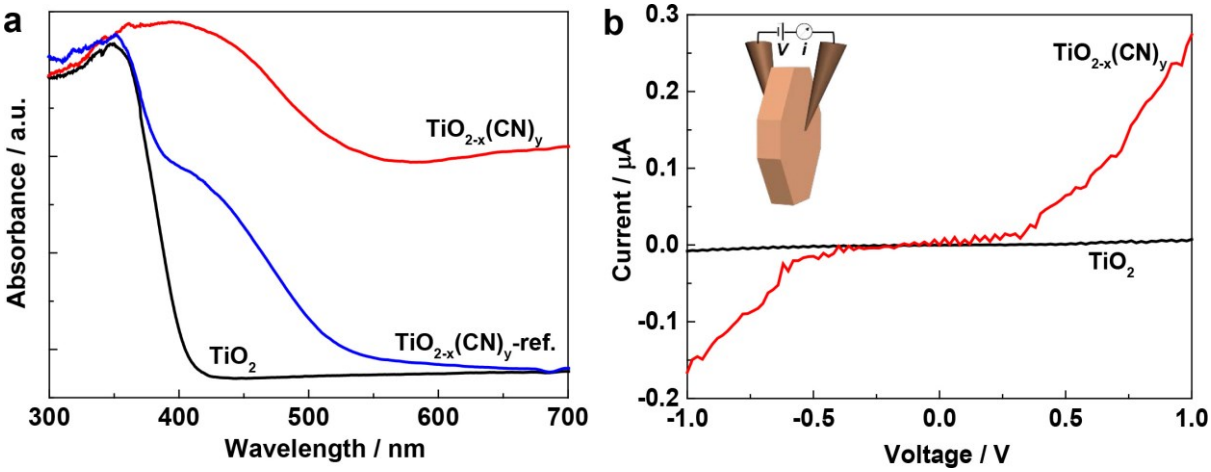

Figure 4. a, UV-visible absorption spectra of three TiO_2 samples (the $TiO_{2-x}(CN)_y$ with the homogeneous doping of nitrogen and carbon, the $TiO_{2-x}(CN)_y$ with the non-homogeneous doping of nitrogen and carbon (denoted as $TiO_{2-x}(CN)_y$-ref.) prepared by heating the $TiO_{2-x}(CN)_y$ sample in air and the undoped TiO_2 sample prepared by the thermal topotactic transition of titanium oxalate hydrate in air); **b**, I-V curves measured from a single particle of $TiO_{2-x}(CN)_y$ or TiO_2. The inset is the schematic of using two tungsten probes as the electrodes to contact the particle to record I-V curves, which was performed in a scanning electron microscope.

The replacement of oxygen with dopants in TiO_2 inevitably causes the formation of some defects to keep the charge balance of the system as a result of their different oxidation states between the dopants and oxygen. The electron spin resonance (ESR) spectrum in Figure 3h

gives two symmetric signals centered at g = 2.003 and 1.987. The strong wide signal at g = 1.987 is assigned to Ti^{3+} defects in the bulk and the weak sharp signal at g = 2.003 is associated with oxygen vacancies in the surface layer.[38-40] The origin of the Ti^{3+} defects is the oxidation state difference between oxygen (O^{2-}) and the substitutional nitrogen (N^{3-}) and carbon (C^{4-}). Surface oxygen vacancies are formed as a result of the loss of some oxygen atoms from TiO_2 in the reductive atmosphere of NH_3 during the topotactic transition.

The great influence of the homogeneous nitrogen and carbon doping and concomitant defects on the optical absorption and electric conductivity of TiO_2 is demonstrated in **Figure 4**. Compared to TiO_2 that has a strong absorption band in UV region before 400 nm, the $TiO_{2-x}(CN)_y$ has an extended band-to-band absorption spectrum up to 500 nm and high background absorption in the whole visible light region. According to the theoretical results reported,[19, 22] the absorption edge extension of $TiO_{2-x}(CN)_y$ is the consequence of the bandgap narrowing caused by the elevation of the valence band maximum with the involvement of N 2*p* and C 2*p* states in O 2*p* states dominated valence band. The high background absorption is caused by the introduction of abundant localized states of Ti^{3+} and oxygen vacancies at the bottom of conduction band and even partially filled conduction band.[18] This allows the effective absorption of photons with very low energies. However, different from the extended intrinsic absorption edge that can make a direct contribution to photocatalysis by providing more photogenerated charge carriers, the background absorption itself cannot generate charge carriers that can be used for photocatalysis. Comparison of the I-V curves of $TiO_{2-x}(CN)_y$ and TiO_2 particles in Figure 4b suggests the greatly increased electric conductivity of the former and also its semiconducting behavior. Several factors, particularly the concentration of carriers and crystallographic orientation,[41] can sensitively affect the electric conductivity of the semiconductor measured. In the present case, the carrier concentration in the $TiO_{2-x}(CN)_y$ sample is increased by a factor of 1.46 from 6.45×10^{19} cm^{-3} to 9.41×10^{19} cm^{-3} as determined from the Mott-Schottky curves of two samples (**Figure S5**, Supporting Information). The

positive slope of both curves suggests the unchanged n-type semiconducting nature of TiO_2 by the homogeneous doping of nitrogen and carbon.

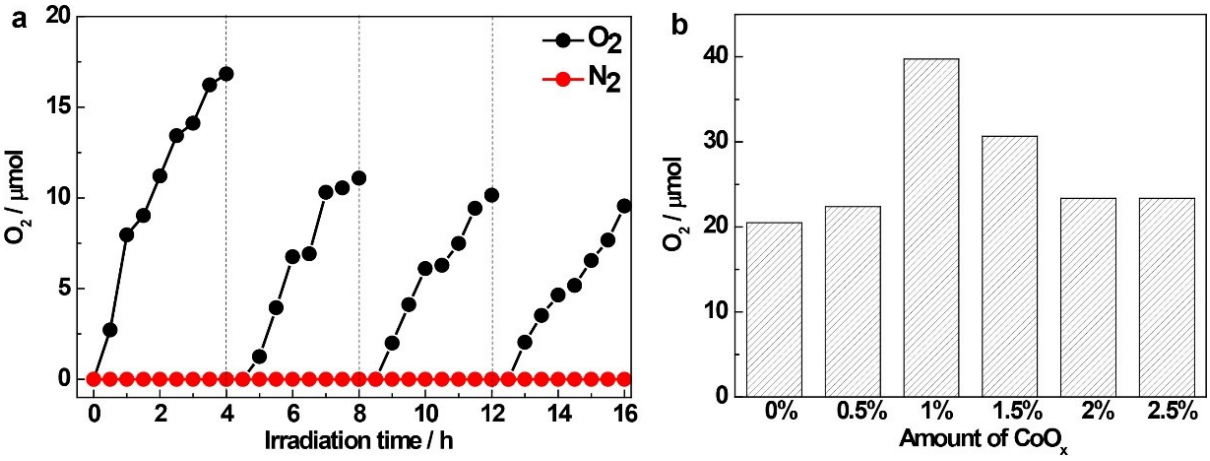

Figure 5. a, Time courses of photocatalytic oxygen evolution from water oxidation in the presence of silver nitrate as a sacrificial agent under visible light irradiation ($\lambda > 420$ nm) with the $TiO_{2-x}(CN)_y$ sample as photocatalyst. **b**, Comparison of photocatalytic oxygen generation from water oxidation with the $TiO_{2-x}(CN)_y$ samples with different amounts of CoO_x cocatalyst.

The increased visible light absorption of the $TiO_{2-x}(CN)_y$ sample makes it a potential visible light responsive photocatalyst. Photocatalytic water oxidation to release oxygen that requires four electrons, which is considered as a central reaction for water splitting, was used to evaluate the activity of the $TiO_{2-x}(CN)_y$ sample as photocatalyst. Photocatalytic oxygen evolution as a function of the visible light irradiation time in **Figure 5**a shows that the $TiO_{2-x}(CN)_y$ can induce water oxidation and gives continuous release of oxygen. The activity decreases in the subsequent cycles should be caused by the photodeposition of Ag from the sacrificial agent on the photocatalyst which partially blocked the incident light to reach the photocatalyst. In contrast, no activity was detected for TiO_2 without visible light absorption. It is remarkable that no nitrogen release as a result of the oxidation of N^{3-} ions by the photogenerated holes, a typical problem that most (oxy)nitrides and nitrogen doped oxides

face, was detected in the photocatalytic reactions. These results suggest the high stability of the $TiO_{2-x}(CN)_y$ sample as photocatalyst. The plausible reason for the high stability is the nitrogen- and carbon-free surface layer of the $TiO_{2-x}(CN)_y$ particles and the location of the dopants in the interior. Loading a suitable cocatalyst is an effective strategy to promote the separation of photogenerated charge carriers and increase catalytically active sites. Figure 5b compares the effect of CoO_x cocatalyst on photocatalytic oxygen generation of the $TiO_{2-x}(CN)_y$ photocatalyst. The optimal amount of 1 wt% CoO_x cocatalyst loaded by chemical impregnation doubles the activity. Further exploration and loading optimization of other cocatalysts might boost the photocatalytic activity greatly.

The significance of the band-to-band visible light absorption in enabling the visible light photocatalytic activity of the $TiO_{2-x}(CN)_y$ sample can be validated by comparing the activity of the reference photocatalyst C/N doped TiO_2 photocatalyst with a shoulder-like visible light absorption band (UV-visible absorption spectrum in Figure 4a, SEM image and XRD pattern in **Figure S7** & **8**, Supporting Information). This reference photocatalyst was prepared by oxidizing the $TiO_{2-x}(CN)_y$ sample in air at 550 ^oC for 2 h to remove some outer dopants and thus form a non-homogeneous N/C doping. No activity in releasing oxygen from photocatalytic water oxidation at the same reaction conditions was observed. This could be understood by their different electronic structures caused by the homogeneous and non-homogeneous doping. The mobility of the photogenerated holes in the localized states of the TiO_2 with a shoulder-like visible light absorption band (non-homogeneous doping) is low, while the mobility of the photogenerated holes in the newly formed valence band in the TiO_2 with the band-to-band visible light absorption (homogeneous doping) is high.

3. Conclusion

In summary, homogeneous doping of substitutional carbon/nitrogen to oxygen in TiO_2 plates with a dominant anatase phase was achieved by thermal topotactic transition of

titanium oxalate hydrate plates in the atmosphere of gaseous ammonia. The resultant $TiO_{2-x}(CN)_y$ sample has a desirable spectrum of strong band-to-band visible light absorption as a result of the homogeneous nitrogen/carbon doping to narrow the bandgap. The success of this preparation strategy lies in that, prior to the completion of the thermal topotactic transition of titanium oxalate hydrate, abundant one-dimensional spaces with rhombus-like cross-sections in its crystal structure can provide favorable channels for the entrance of NH_3 molecules and their derivatives during thermal decomposition into the material interior. Moreover, the $TiO_{2-x}(CN)_y$ sample as a stable photocatalyst has the ability of inducing water oxidation to release oxygen under visible light irradiation.

4. Experimental Section

Sample preparation: A titanium oxalate hydrate sample was prepared by the aqueous precipitation reaction of titanium oxysulfate ($TiOSO_4 \cdot H_2O$) as a titanium precursor and lithium oxalate ($Li_2C_2O_4$) as a ligand stabilizer, according to the modified procedures[35, 36]. To prepare the $TiO_{2-x}(CN)_y$ sample, the titanium oxalate hydrate sample obtained was heated at 550 ^oC in a tube furnace in an atmosphere of gaseous ammonia with the flux of 10 mL min^{-1} for 2 h. In the preparation of the reference TiO_2 sample, the titanium oxalate hydrate sample was heated at 550 ^oC in air for 2 h. To prepare the CoO_x cocatalyst modified $TiO_{2-x}(CN)_y$ sample, the titanium oxalate hydrate sample was first chemically impregnated with $Co(NO_3)_2$ and subsequently subjected to the thermal topotactic transition at 550 ^oC in a tube furnace in an atmosphere of gaseous ammonia with the flux of 10 mL min^{-1} for 2 h.

Details for the characterizations of the samples and photocatalytic water oxidation measurement are provided in Supporting Information.

Supporting Information

Supporting Information is available from the Wiley Online Library or from the authors.

Acknowledgements

The authors thank National Natural Science Foundation of China (Nos. 51825204， 51572266, 21633009, 51629201), the Key Research Program of Frontier Sciences CAS (QYZDB-SSW-JSC039) for the financial support. G. L. is grateful for the award of the Newton Advanced Fellowship.

Received: ((will be filled in by the editorial staff))
Revised: ((will be filled in by the editorial staff))
Published online: ((will be filled in by the editorial staff))

[1] S. S. Chen, T. Takata, K. Domen, *Nat. Rev. Mater.*, **2017**, *2*, 17050.

[2] C. Y. Toe, Z. K. Zheng, H. Wu, J. Scott, R. Amal, Y. H. Ng, *Angew. Chem. Int. Ed.*, **2018**, *57*, 13613.

[3] Q. M. Sun, N. Wang, J. H. Yu, J. C. Yu, *Adv. Mater.*, **2018**, *30*, 1804368.

[4] Q. Wang, T. Hisatomi, Q. X. Jia, H. Tokudome, M. Zhong, C. Z. Wang, Z. H. Pan, T. Takata, M. Nakabayashi, N. Shibata, Y. B. Li, I. D. Sharp, A. Kudo, T. Yamada, K. Domen, *Nat. Mater.*, **2016**, *15*, 611.

[5] K. Kawashima, M. Hojamberdiev, H. Wagata, M. Nakayama, K. Yubuta, S. Oishi, K. Domen and K. Teshima, *Catal. Sci. & Technol.*, **2016**, *6*, 5389.

[6] K. Iwashina, A. Iwase, A. Kudo, *Chem. Sci.*, **2015**, *6*, 687.

[7] Y. Yamaguchi, S. Usuki, K. Yamatoya, N. Suzuki, K. Katsumata, C. Terashima, A. Fujishima, A. Kudo, K. Nakata, *Rsc Adv.*, **2018**, *8*, 5331.

[8] A. Miyoshi, J. J. M. Vequizo, S. Nishioka, Y. Kato, M. Yamamoto, S. Yamashita, T. Yokoi, A. Iwase, S. Nozawa, A. Yamakata, T. Yoshida, K. Kimoto, A. Kudo, K. Maeda, *Sustainable Energy & Fuels*, **2018**, *2*, 2025.

[9] A. Iwase, S. Yoshino, T. Takayama, Y. H. Ng, R. Amal, A. Kudo, *J. Am. Chem. Soc.*, **2016**, *138*, 10260.

[10] A. Iwase, A. Kudo, *Chem. Commun.*, **2017**, *53*, 6156.

[11] Y. T. Wang, J. M. Cai, M. Q. Wu, H. Zhang, M. Meng, Y. Tian, T. Ding, J. L. Gong, Z. Jiang, X. G. Li, *Acs Appl. Mater. & Interface*, **2016**, *8*, 23006.

[12] C. C. Li, T. Wang, Z. B. Luo, S. S. Liu, J. L. Gong, *Small*, **2016**, *12*, 3415.

[13] W. J. Ong, L. L. Tan, Y. H. Ng, S. T. Yong, S. P. Chai, *Chem. Rev.*, **2016**, *116*, 7159.

[14] R. G. Li, F. X. Zhang, D. G. Wang, J. X. Yang, M. R. Li, J. Zhu, X. Zhou, H. X. Han, C. Li, *Nat. Commun.*, **2013**, *4*, 1432.

[15] F. E. Osterloh, *J. Phys. Chem. Lett.*, **2014**, *5*, 2510.

[16] S. S. Chen, Y. Qi, T. Hisatomi, Q. Ding, T. Asai, Z. Li, S. S. K. Ma, F. X. Zhang, K. Domen, C. Li, *Angew. Chem. Int. Ed.*, **2015**, *54*, 8498.

[17] T. Oshima, T. Ichibha, K. S. Qin, K. Muraoka, J. J. M. Vequizo, K. Hibino, R. Kuriki, S. Yamashita, K. Hongo, T. Uchiyama, K. Fujii, D. L. Lu, R. Maezono, A. Yamakata, H. Kato, K. Kimoto, M. Yashima, Y. Uchimoto, M. Kakihana, O. Ishitani, H. Kageyama, K. Maeda, *Angew. Chem. Int. Ed.*, **2018**, *57*, 8154.

[18] Y. Q. Yang, L. C. Yin, Y. Gong, P. Niu, J. Q. Wang, L. Gu, X. Q. Chen, G. Liu, L. Z. Wang, H. M. Cheng, *Adv. Mater.*, **2018**, *30*, 1704479.

[19] R. Asahi, T. Morikawa, H. Irie, T. Ohwaki, *Chem. Rev.*, **2014**, *114*, 9824.

[20] X. C. Wang, K. Maeda, A. Thomas, K. Takanabe, G. Xin, J. M. Carlsson, K. Domen, M. Antonietti, *Nat. Mater.*, **2009**, 8, 76.

[21] X. X. Xu, C. Randorn, P. Efstathiou, J. T. S. Irvine, *Nat. Mater.*, **2012**, *11*, 595.

[22] R. Asahi, T. Morikawa, T. Ohwaki, K. Aoki, Y. Taga, *Science*, **2001**, *293*, 269.

[23] G. Liu, L.-C. Yin, J. Wang, P. Niu, C. Zhen, Y. Xie, H.-M. Cheng, *Energy & Environ. Sci.*, **2012**, *5*, 9603.

[24] W. Zhao, W. H. Ma, C. C. Chen, J. C. Zhao, Z. G. Shuai, *J. Am. Chem. Soc.*, **2004**, *126*, 4782.

[25] N. Serpone, *J. Phys. Chem. B*, **2006**, *110*, 24287.

[26] J. H. Lee, D. Fernandez Hevia, A. Selloni, *Phys. Rev. Lett.*, **2013**, *110*, 016101.

[27] T. M. Breault, B. M. Bartlett, *J. Phys. Chem. C*, **2012**, *116*, 5986.

[28] K. S. Yang, Y. Dai, B. B. Huang, M. H. Whangbo, *J. Phys. Chem. C*, **2009**, *113*, 2624.

[29] G. Liu, L. Wang, C. Sun, X. Yan, X. Wang, Z. Chen, S. C. Smith, H.-M. Cheng, G. Q. Lu, *Chem. Mater.*, **2009**, *21*, 1266.

[30] X. Hong, J. Tan, H. Zhu, N. Feng, Y. Yang, J. T. S. Irvine, L. Wang, G. Liu, H.-M. Cheng, *Chem-A Europ. J.*, **2019**, *25*, 1787.

[31] H. Irie, Y. Watanabe, K. Hashimoto, *J. Phys. Chem. B*, **2003**, *107*, 5483.

[32] G. Liu, L. Z. Wang, H. G. Yang, H. M. Cheng, G. Q. Lu, *J. Mater. Chem.*, **2010**, *20*, 831.

[33] G. Liu, C. Zhen, Y. Y. Kang, L. Z. Wang, H. M. Cheng, *Chem. Soc. Rev.*, **2018**, *47*, 6410.

[34] Y. Y. Kang, Y. Q. Yang, L. C. Yin, X. D. Kang, L. Z. Wang, G. Liu, H. M. Cheng, *Adv. Mater.*, **2016**, *28*, 6471.

[35] D. Dambournet, I. Belharouak, K. Amine, *Chem. Mater.*, **2010**, *22*, 1173.

[36] P. Niu, T. T. Wu, L. Wen, J. Tan, Y. Q. Yang, S. J. Zheng, Y. Liang, F. Li, J. T. S. Irvine, G. Liu, X. L. Ma, H. M. Cheng, *Adv. Mater.*, **2018**, *30*, 1705999.

[37] H.-L. Choi, N. Enomoto, N. Ishizawa, Z. Nakagawa, *Powder Diffraction*, **1994**, *9*, 187.

[38] I. Nakamura, N. Negishi, S. Kutsuna, T. Ihara, S. Sugihara, E. Takeuchi, *J. Mol. Catal. A-Chem.*, **2000**, *161*, 205.

[39] M. Anpo, T. Shima, S. Kodama, Y. Kubokawa, *J. Phys. Chem.*, **1987**, *91*, 4305.

[40] Y. Nakaoka, Y. Nosaka, *J. Photochem. Photobio. A-Chem.*, **1997**, *110*, 299.

[41] G. Liu, L.-C. Yin, J. Pan, F. Li, L. Wen, C. Zhen, H.-M. Cheng, *Adv. Mater.*, **2015**, *27*, 3507.